MOLECULAR AND CELLULAR BIOLOGY, Nov. 2005, p. 10087–10096 Vol. 25, No. 22
0270-7306/05/$08.00+0 doi:10.1128/MCB.25.22.10087–10096.2005

Caveolin-1 Is Not Essential for Biosynthetic Apical Membrane Transport

Aki Manninen,[1] Paul Verkade,[1] Soazig Le Lay,[1] Juha Torkko,[1] Michael Kasper,[3] Joachim Füllekrug,[2] and Kai Simons[1]*

Max Planck Institute of Molecular Cell Biology and Genetics, 01307 Dresden, Germany[1]; University of Heidelberg, Im Neuenheimer Feld 345, 69120 Heidelberg, Germany[2]; and Institute of Anatomy, Medical Faculty Carl Gustav Carus, Dresden University of Technology, Fiedlerstrasse 42, 01307 Dresden, Germany[3]

Received 30 May 2005/Returned for modification 10 July 2005/Accepted 28 August 2005

Caveolin-1 has been implicated in apical transport of glycosylphosphatidylinositol (GPI)-anchored proteins and influenza virus hemagglutinin (HA). Here we have studied the role of caveolin-1 in apical membrane transport by generating caveolin-1-deficient Madin-Darby canine kidney (MDCK) cells using retrovirus-mediated RNA interference. The caveolin-1 knockdown (cav1-KD) MDCK cells were devoid of caveolae. In addition, caveolin-2 was retained in the Golgi apparatus in cav1-KD MDCK cells. However, we found no significant alterations in the apical transport kinetics of GPI-anchored proteins or HA upon depletion of caveolin-1. Similar results were obtained using embryonic fibroblasts from caveolin-1-knockout mice. Thus, we conclude that caveolin-1 does not play a major role in lipid raft-mediated biosynthetic membrane trafficking.

The plasma membrane of polarized epithelial cells is segregated into two distinct domains, the apical and basolateral membranes, separated by tight junctions. The apical surface faces the lumenal space, whereas the basolateral surface is formed between the neighboring cells and the underlying basal lamina. Communication with the environment at these two interfaces requires different machineries and therefore the protein and lipid compositions of the apical and basolateral membranes are different. This polarity is established and maintained by dynamic membrane trafficking and signaling networks (11, 36, 39, 53, 58).

Polarized membrane trafficking is mediated by specific sorting determinants on the cargo proteins. Tyrosine- and dileucine-based amino acid motifs located on the cytoplasmic domains govern the targeting of basolateral membrane proteins (38). Apical signals seem to be more diverse. Apical targeting information has been located to lipid modifications, transmembrane domains, N- and O-glycans as well as to cytoplasmic or exoplasmic short amino acid motifs (36, 53, 58).

According to the current models of protein sorting at the trans-Golgi network, the assembly of adaptor-protein complexes drives the formation of basolateral transport containers, whereas clustering of lipid rafts into sorting platforms generates apical transport carriers (53, 58). Lipid rafts are sphingolipid- and cholesterol-based liquid-ordered membrane microdomains which are able to recruit and exclude proteins and lipids based on their physicochemical properties (59). Although the important role of raft domains in apical sorting is recognized, the protein machinery and the clustering mechanism operating at the trans-Golgi network are not understood.

The lipid raft model relies on raft organizer proteins which cross-link raft components. A putative lectin cross-linker has been proposed to cluster rafts at the trans-Golgi network by binding to glycoproteins and/or glycolipids (19). Such a role has been suggested for VIP36, although its localization is restricted to the early secretory pathway (18, 22). In addition, galectin-4 was recently shown to be required for efficient surface delivery of apical proteins in enterocyte-like cells (7). An alternative way to cluster rafts would be via homo- or hetero-oligomerization of raft-resident proteins. For example, VIP17/MAL (5, 50) and MAL2 (8), two members of the large tetraspanin family, and annexin 13b (12, 27), a member of the annexin family of proteins, have been implicated in apical transport, although their mechanistic roles have not been fully elucidated.

Caveolins are cholesterol-binding integral membrane proteins which acquire raft association while forming high-molecular-weight complexes during their transport along the secretory pathway (34, 37, 56). At the plasma membrane, oligomerized caveolin-1, typically as a hetero-oligomer together with the related caveolin-2, constitute a scaffold for a specialized invaginated raft domain-forming caveolae (17, 54). These membrane structures can function as transport carriers and as signaling platforms (6, 31, 45). The proposed role of caveolin-1 in biosynthetic apical trafficking stems from a series of observations. (i) Caveolin-1 (VIP21) was identified from two sources, trans-Golgi network-derived vesicular preparation from polarized epithelial cells (25) and caveolae (54). (ii) Application of caveolin-1 antibodies into permeabilized Madin-Darby canine kidney (MDCK) cells inhibited apical (influenza virus hemagglutinin) but not basolateral (vesicular stomatitis virus G protein) transport (56). (iii) More recently, severe defects were reported in the surface delivery of glycosylphosphatidylinositol (GPI)-anchored proteins in immortalized mouse embryonic fibroblasts (MEFs) derived from caveolin-1-knockout (cav1-KO) mice (60). Nonetheless, such an essential role for caveolin-1 in raft-mediated membrane trafficking has

* Corresponding author. Mailing address: Max Planck Institute of Molecular Cell Biology and Genetics, Pfotenhauerstrasse 108, 01307 Dresden, Germany. Phone: 49-351-210 2800. Fax: 49-351-210 2900. E-mail: simons@mpi-cbg.de.

been challenged by the relatively mild phenotypes reported for cav1-KO mice (10, 52).

Here we have clarified the role of caveolin-1 in apical transport by characterizing caveolin-1-deficient MDCK cells generated using a retrovirus-mediated RNA interference (RNAi)-methodology. This approach allows us to follow the effects of caveolin-1 depletion in a well-characterized polarized cell model. Importantly, by following retrovirus-transduced populations of caveolin-1-knockdown (cav1-KD) cells shortly after the loss of caveolin-1 expression, we minimize any bias resulting from lengthy selection procedures for producing stable transfectants. In agreement with the essential role of caveolin-1 in the biogenesis of caveolae, we found that cav1-KD MDCK cells lacked caveolae. In addition, the localization of caveolin-2 at the plasma membrane was perturbed and it accumulated in the Golgi complex instead. However, the surface expression of a number of other polarized membrane markers was normal in cav1-KD cells. Moreover, the kinetics of biosynthetic apical transport of the influenza virus hemagglutinin (HA) and the GPI-anchored marker proteins were similar in control and in caveolin-1-depleted cells. Our results strongly suggest that caveolin-1 found in apical transport carriers is there as a cargo and not as an essential component of the raft-based apical transport machinery.

MATERIALS AND METHODS

Antibodies and expression constructs. The polyclonal caveolin-1 N20 antibody was from Santa Cruz Biotechnology. Mouse monoclonal antibodies against placental alkaline phosphatase (PLAP) (62), E-cadherin (21), gp114 and gp58 (2), and rabbit polyclonal antibody against caveolin-2 (56) were raised in our laboratory. The hybridoma cell line 3F2 secreting antibody against gp135/podocalyxin (41), was provided by G. Ojakian (State University of New York Downstate Medical Center, Brooklyn, NY) and A. Muesch (Cornell University, Ithaca, NY). Mouse antigiantin antibody (29) was a kind gift from H. P. Hauri (Biozentrum, University of Basel, Switzerland). Alexa-546-conjugated aerolysin mutant (Alexa-546-ASSP) (14) was provided by F. G. van der Goot (University of Geneva, Switzerland). Mouse antitransferrin antibody was purchased from Zymed (Zymed Laboratories Inc.). Rabbit anti-Tamm-Horsfall protein antibody was from Chemicon (Chemicon Europe). Secondary antibodies were from Jackson Immunoresearch Laboratories Inc.

A full-length cDNA of canine caveolin-2 was obtained from an MDCK cDNA library and fused to the 3′ end of enhanced green fluorescent protein (EGFP) cDNA to generate a green fluorescent protein (GFP)-cav2 fusion construct. The GFP-cav2 fusion construct and PLAP cDNA (a kind gift from D. Brown) (4) were subcloned into the pShuttle-CMV expression vector (Stratagene). Recombinant adenoviruses were generated using the AdEasy adenoviral system (Stratagene) according to the manufacturer's instructions.

Cell culture. MDCK strain II and MDCK II-PLAP cells were maintained in Earle's minimal essential medium (PAA Laboratories) supplemented with 2 mM L-glutamine (Gibco BRL, Invitrogen), 100 U/ml penicillin, 100 μg/ml streptomycin (Gibco BRL) and 5 to 10% fetal calf serum (PAA Laboratories). Mouse embryonic fibroblasts were prepared from 13.5-day postcoitus embryos obtained by homozygous crossing of wild-type or cav1-KO mice. Primary cells were grown in Dulbecco's modified Eagle's medium with high glucose (Gibco BRL) supplemented with L-glutamine, penicillin/streptomycin, and 10% fetal calf serum. MEFs were immortalized by passaging them continuously, according to the 3T3 protocol, until the growth rates of immortalized cells reached the rates of early-passage (<5) primary cells. The Phoenix gag-pol retroviral packaging cell line (http://www.stanford.edu/group/nolan/retroviral_systems/phx.html; obtained from the American Type Culture Collection with authorization by Garry Nolan, School of Medicine, Stanford University, Stanford, CA) was kept in high-glucose Dulbecco's modified Eagle's medium (Gibco BRL) containing L-glutamine, penicillin/streptomycin, and 10% fetal calf serum.

Generation of caveolin-1-KD cells by retrovirus-mediated RNAi. A target sequence (AAG ATG TGA TTG CAG AAC CAG) corresponding to nucleotides 206 to 226 of canine caveolin-1 coding sequence (gi:50979109) was selected. Annealed oligonucleotides (Cav1-KD-sense: 5′-GAT CCC CGA TGT GAT TGC AGA ACC AGT TCA AGA GAC TGG TTC TGC AAT CAC ATC TTT TTG GAA A-3′; Cav1-KD antisense: 5′-AGC TTT TCC AAA AAG ATG TGA TTG CAG AAC CAG TCT CTT GAA CTG GTT CTG CAA TCA CAT CGG G-3′; Sigma Genosys) were cloned into an RVH-1-puro retroviral vector and recombinant knockdown viruses were generated as described previously (57). Subconfluent MDCK strain II cells were trypsinized and 5×10^5 cells in 3 ml of complete MEM (5% fetal calf serum) supplemented with 4 μg/ml of hexadimethrine bromide (Polybrene, Sigma) were seeded onto a 3.5-cm-diameter culture dish (Corning Costar). On the next day, medium was aspirated and 1 ml of control or cav1-KD virus-containing precleared supernatant from Phoenix cells was added. Hexadimethrine bromide (4 μg/ml) was added to virus preparations before use. One hour later 1 ml of fresh complete MEM (5% fetal calf serum) was added and incubation was continued for 8 to 12 h. Infection was repeated once, after which cells were trypsinized and reseeded into MEM containing 4 μg/ml of puromycin (BD Biosciences) to select retrovirus-transduced cells (transduction efficiency was 50 to 80%). Maximum knockdown efficiencies were obtained after 2 to 3 days of puromycin selection and the resulting stable KD cell populations were used for experiments for up to 2 weeks without any significant drop in the knockdown efficiency. Knockdown efficiency during the culturing of the KD cells was analyzed by reverse transcription-PCR as described previously (57).

Adenoviral infection. MDCK II cells grown on 12-mm Transwell filters were washed twice with PBS^- (phosphate-buffered saline without Ca^{2+} and Mg^{2+}) and incubated for 10 min in PBS^-. Three to five microliters of OPTIPREP (Axis-Shield) gradient-purified adenovirus in adenovirus storage buffer (5 mM Tris pH 8.0, 50 mM NaCl, 0.05% bovine serum albumin, 60% glycerol) was diluted to 150 μl with OPTIMEM (Gibco BRL) supplemented with L-glutamine. Virus was added onto apical side (basolateral side was left empty), cells incubated at 37°C for 1 h followed by an addition of 500 μl and 1500 μl of complete MEM to apical and basolateral chambers, respectively.

Plastic grown cells were washed once with OPTIMEM supplemented with L-glutamine, virus was added in a small volume of OPTIMEM, cells incubated at 37°C for 1 h, and finally complete medium was added.

Electron microscopy. We punched 1.5-mm circles from polarized filter grown cells. They were immersed and rapidly frozen in 20% bovine serum albumin in medium using an EMPACT2+RTS high-pressure freezing system (Leica Microsystems). This machine contains an automatic transfer system to facilitate loading and freezing and hence gives very reproducible results. The frozen samples were freeze-substituted in acetone containing 1% osmium tetroxide and 0.1% uranyl acetate using an automatic freeze substitution (Leica Microsystems) and afterwards embedded in Epon. Ultrathin sections were counterstained according to standard procedures. Immunoelectron microscopy was performed as described previously (56). Caveolae were quantified on immunolabeled sections mainly based on the criteria described in (28). To distinguish caveolae from other membrane invaginations, we added a more stringent criterion, namely that a caveolar profile that was open to the plasma membrane also had to be immunolabeled for caveolin-1.

Immunofluorescence microscopy. For immunofluorescence, MDCK II cells were washed once with PBS containing 0.9 mM Ca^{2+} and 0.5 mM Mg^{2+} (PBS^+) and fixed by incubating for 20 min in PBS containing 4% paraformaldehyde (Sigma). After one wash with PBS, remaining paraformaldehyde was quenched by incubating cells for 20 min in PBS/200 mM glycine (Sigma). When indicated, cells were permeabilized either in PBS/0.1% Triton X-100 (Sigma) or PBS/0.1% saponin (Sigma) for 10 min. Nonspecific binding was blocked in PBS/0.1% fish skin gelatin (Sigma)/0.5% bovine serum albumin (Sigma) for 20 min.

Cells were incubated 45 min with primary antibodies (diluted 1:100 into blocking solution for anti-cav-1, gp58, PLAP, giantin, and podocalyxin, 1:50 for anti-E-cadherin and gp114), washed extensively in PBS, incubated 30 min with 1:500 dilutions of fluorophore-conjugated secondary antibodies, washed in PBS, and mounted on slides with Moviol. Images were acquired with either Leica TCS SP2 (Leica Microsystems; using a 63X HCX PL APO oil immersion objective NA 1.32) or Zeiss LSM 510 (Carl Zeiss Inc.; using a 63× C-Apochromat water immersion objective NA 1.2 or a 100× Plan Apochromat oil, NA 1.4) laser scanning confocal microscopes.

Immunohistochemistry. Four-micron-thick paraffin sections, layered on silane-coated slides, were used for immunohistochemical staining with primary rabbit antibodies against Tamm-Horsfall protein (diluted 1:400). Prior to immunostaining using the Vectastain Elite kit (Vector/Alexis, Grunberg, Germany), the sections were treated with 10 mM sodium citrate buffer (pH 6.0) in a microwave (750 W, twice for 5 min each). Endogenous peroxidase in the tissue was blocked by incubation in PBS containing 1% H_2O_2. Nonspecific binding sites were blocked with 10% goat serum in PBS (15 min at room temperature). Following the incubation with the primary antibody (1 h, 37°C), the sections were

washed with PBS and incubated with the biotinylated secondary antibody (30 min, 37°C) and with the ABC complex (30 min, 37°C). Following further washes with PBS, bound ABC complexes were detected with 0.06% diaminobenzidine tetrahydrochloride in PBS. The sections were counterstained with hematoxylin. Controls for immunospecificity were included in all experiments by omission of the primary antibody and its replacement by phosphate-buffered saline and matching concentrations of normal rabbit serum (data not shown).

Trans-Golgi network-to-surface transport of influenza virus hemagglutinin. The transport assay to detect the surface arrival of fowl plague virus hemagglutinin (HA) by trypsin cleavage was performed as previously described (32, 64). Briefly, control and cav1-KD cells, grown for 3 days on 12-mm Transwell filters, were infected with fowl plague virus. Four hours later, cells were washed twice with PBS^+, once with starvation medium (EMEM without methionine and cysteine, PAA Laboratories), followed by 15 min incubation in starvation medium. Cells were pulsed with 20 μCi of [^{35}S]methionine for 8 min, washed and incubated at 19.5°C for 75 min to accumulate the biosynthetic cargo at the trans-Golgi network, and finally chased for the indicated times at 37°C. Apical surface-exposed HA was cleaved by adding trypsin (0.1 mg/ml) to the apical side and incubating on ice for 30 min. Soybean trypsin inhibitor (1 mg/ml) was added followed by 5 min incubation, two PBS^+ washes, and cell lysis in TNE lysis buffer (10 mM Tris-HCl pH 7.4, 150 mM NaCl, 5 mM EDTA, 2% NP-40). Full-length and cleaved HA bands were separated on sodium dodecyl sulfate (SDS)-polyacrylamide gel electrophoresis (PAGE) and quantified using a Fuji BAS-1800 phosphorimager. The apical transport index is determined with the equation [apically cleaved HA/(full-length HA + apically cleaved HA)].

Cell surface biotinylation of PLAP. MDCK II cells grown in 12-mm Transwell filters were washed twice with PBS^+ and once with starvation medium followed by 15 min incubation in starvation medium. Cells were labeled for 20 min with 20 μCi of [^{35}S]methionine (Amersham Biosciences) and chased for the indicated times. After washing with ice-cold PBS^+ cell surface biotinylation was performed on ice for 1 h in 0.5 mg/ml of sulfo-NHS-LC-biotin (Pierce) in PBS^+. Cells were quenched with two incubations in MEM complete (5% fetal calf serum), washed in PBS^+ and lysed in TNE lysis buffer. PLAP was immunoprecipitated from the cleared lysate using 2 μl of polyclonal PLAP antibody followed by addition of protein G-Sepharose beads. Immunocomplexes were washed three times with lysis buffer and disrupted by boiling for 2 min in 80 μl of lysis buffer containing 1% SDS. Samples were diluted to 800 μl and biotinylated proteins were precipitated using streptavidin-Sepharose beads (Roche Diagnostics). Samples were subjected to SDS-PAGE, gels were dried and surface exposed, and total PLAP signals were quantified using a phosphorimager.

RESULTS

Retrovirus-mediated RNAi of caveolin-1 in MDCK cells. To clarify the role of caveolin-1 in apical transport in MDCK cells we generated cav1-KD MDCK cells by using a retrovirus-mediated RNAi method recently set up in our laboratory (57). In the resulting cav1-KD MDCK cell population, the caveolin-1 mRNA expression was reduced by 90 to 95%, as measured by real-time PCR. In agreement with the observed mRNA depletion, the protein levels of caveolin-1 in cav1-KD cells were about 5% of those expressed in control cells (Fig. 1). MDCK cells infected with a retrovirus containing an empty short hairpin RNA expression cassette were used as a control in most experiments. To ensure that expression of a short hairpin RNA per se does not induce any nonspecific effects, an additional control virus was used in some experiments (for example, ultrastructural analysis by electron microscopy). This control virus expressed an short hairpin RNA targeted against another cellular protein than caveolin-1. No differences were observed between these two control cell populations in any of the assays used.

In previous studies in caveolin-1 knockout (cav1-KO) mice, a concomitant strong decrease in the caveolin-2 protein levels was observed (10, 52). We also noted a reduction in the caveolin-2 protein levels in cav1-KD MDCK cells (Fig. 1). The mRNA levels of caveolin-2 were not affected in cav1-KD

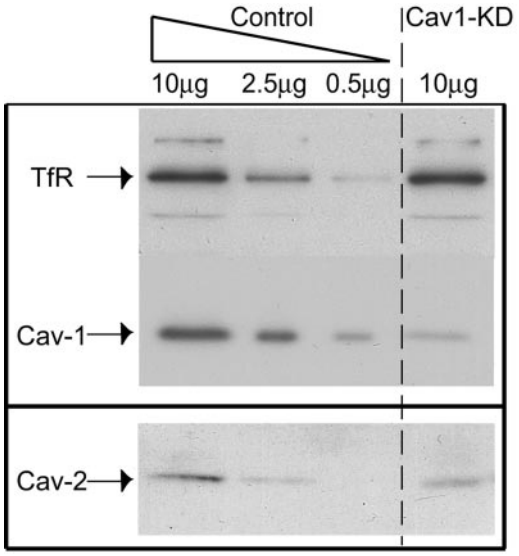

FIG. 1. Depletion of caveolin-1 expression in MDCK cells by retrovirus-mediated RNAi. (A) Lysates from puromycin-selected control and cav1-KD cells were analyzed for expression of caveolin-1. Transferrin receptor (TfR) was used as a loading control. Two dilutions of the control lysate (25% and 5% of total) were loaded to allow an estimation of the remaining caveolin-1 protein levels in cav1-KD cells. (B) Expression of caveolin-2 in control and in cav1-KD cells. The data shown is representative of several independent experiments.

MDCK cells (data not shown) indicating that the down-regulation of caveolin-2 protein expression was due to a posttranslational effect as reported previously (10, 52).

Cav-1 depleted MDCK cells lack caveolae but are able to polarize. MDCK cells are one of the best-studied polarized cell models whose morphology and polarized characteristics have been extensively delineated. To analyze the cav1-KD MDCK cells further, we next examined the ultrastructure of filter-grown (3 days) cells by electron microscopy. Numerous caveolar structures, either with an opening to the plasma membrane or located just underneath the surface, were readily visible at the lateral membranes of control cells (Fig. 2A). On the contrary, cav1-KD MDCK cells were almost devoid of such structures (Fig. 2A).

Because cav1-KD cells still expressed low levels of caveolin-1, it could be possible that these remaining caveola-like profiles were real caveolae. To further investigate this we performed a quantitative immunoelectron microscopy for caveolin-1. To unequivocally assign a caveola-like invagination as a caveola we only quantitated those profiles that also contained label for caveolin-1 (Fig. 2B).

Although caveolae were frequently detected in the control cells, none were found in the cav1-KD cells (Fig. 2B). These findings are in agreement with the reported role of caveolin-1 as an essential component of the caveolar coat (10, 35, 43, 52) and that certain threshold levels of caveolin-1 protein are required for formation of caveolae (15). Although caveolae were absent, the cav1-KD MDCK cells had otherwise a normal polarized phenotype as assessed by the general ultrastructural analysis. Cav1-KD cells were as tall as the control cells (~10 to 12 μm) and had morphologically normal tight junctions (data not shown).

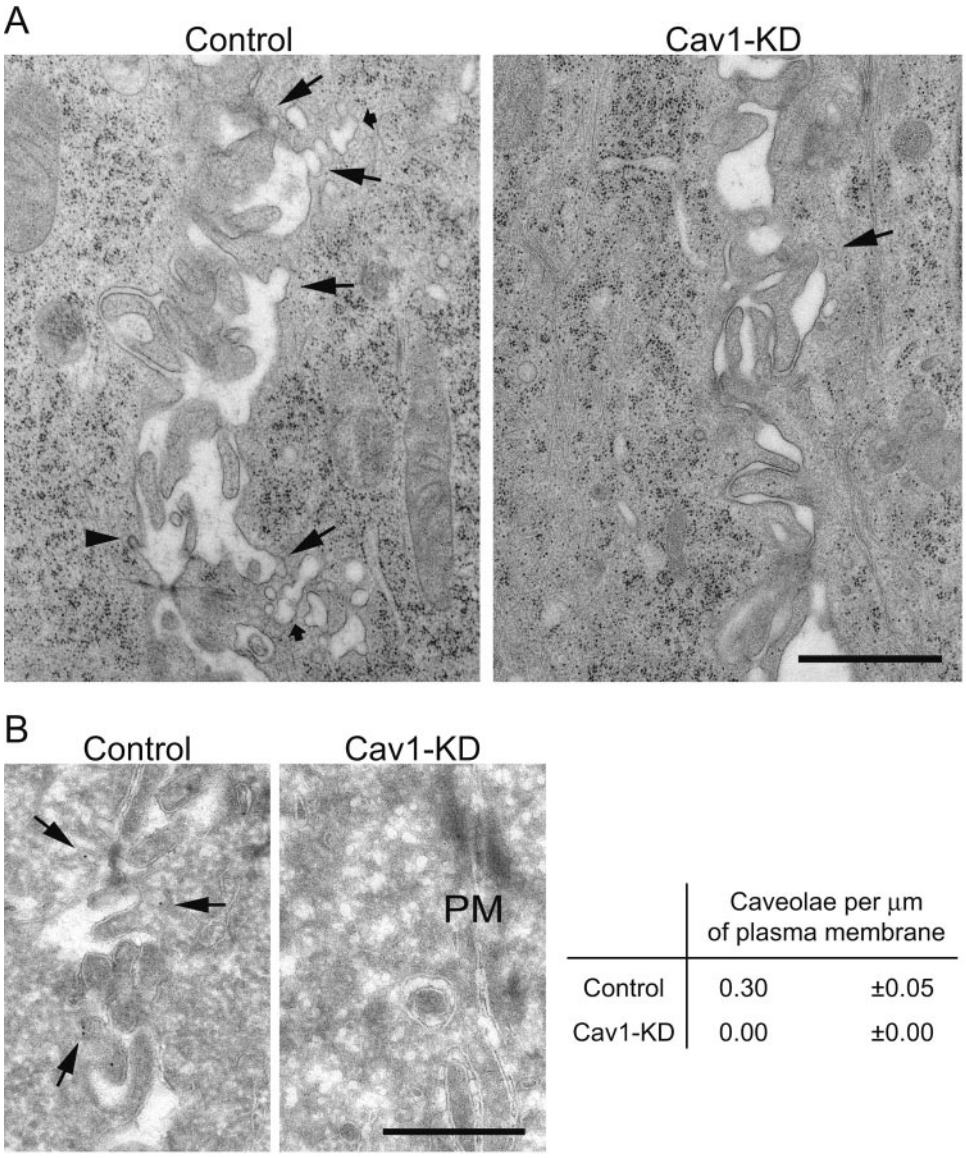

	Caveolae per μm of plasma membrane	
Control	0.30	±0.05
Cav1-KD	0.00	±0.00

FIG. 2. Cav1-KD MDCK cells lack caveolae. (A) Electron micrographs of the basolateral membrane of control and cav1-KD MDCK cells. Control cells displayed several caveolar profiles open to the plasma membrane (big arrows) and just underneath the plasma membrane (small arrows). Cav1-KD cells, on the contrary, only seldom displayed an uncoated membrane invagination (big arrow). Arrowhead points to a clathrin-coated invagination. (B) Electron micrographs of immunolabeling for caveolin-1 and quantitation of the caveolae open to the plasma membrane in control and in cav1-KD cells. In control cells, caveolin-1 label was found on caveola-like invaginations at the plasma membrane. In cav-1 KD cells, no labeling of plasma membrane invaginations was observed. The number of caveolae per μm membrane length is depicted (mean ± standard error of the mean). PM = plasma membrane. Scale bar = 1 μm in A, 500 nm in B.

To examine the polarity of filter-grown cav1-KD cells in more detail, we analyzed the steady-state distribution of selected membrane markers. As basolateral markers we used gp58 and E-cadherin and as apical markers we used gp114 and podocalyxin/gp135 (33) in MDCK cells and placental alkaline phosphatase (PLAP) in MDCK-PLAP cells stably expressing GPI-anchored PLAP. All of these markers were correctly localized to their target membranes (Fig. 3). Thus, no gross defects were observed in the overall polarity of cav1-KD MDCK cells.

Caveolin-2 accumulates in the Golgi apparatus in cav1-KD MDCK cells. The surface delivery of caveolin-2 has been reported to depend on caveolin-1 function. In the absence of caveolin-1, caveolin-2 is retained intracellularly (35, 43). Exogenous expression of caveolin-1 in these cells results in plasma membrane targeting of caveolin-2. In addition, overexpression of a dominant-negative mutant of caveolin in MDCK cells inhibits the surface transport of caveolin-2 (28). Therefore, we examined whether caveolin-2 localization was affected in cav1-KD MDCK cells. In control cells, endogenous caveolin-2 was found at the plasma membrane and at the perinuclear region close to, but distinct from, the Golgi apparatus (Fig. 4A).

In the cav1-KD MDCK cells, on the other hand, the vast

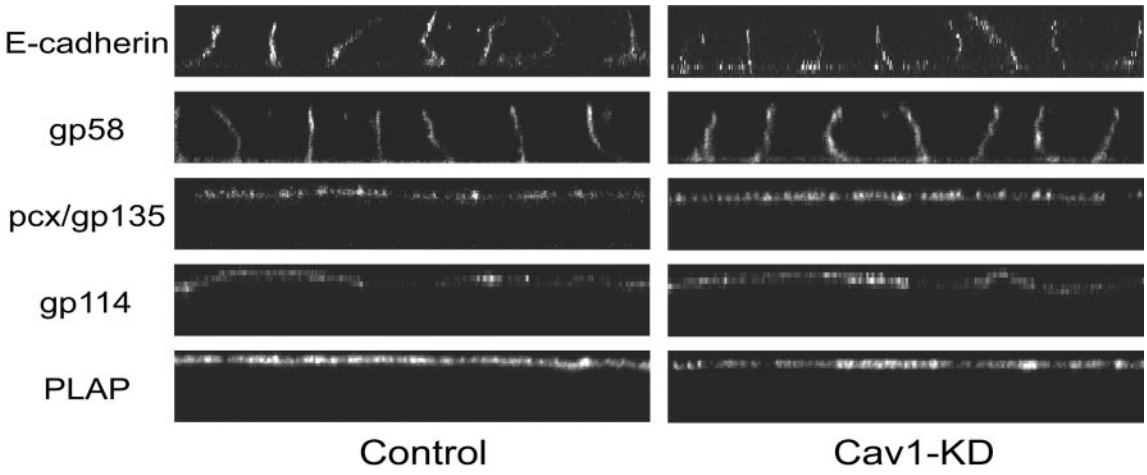

FIG. 3. Confluent cav1-KD MDCK cells form a polarized monolayer. Three-day-old filter-grown cultures of control and cav1-KD MDCK cells or MDCK-PLAP cells were fixed and permeabilized with Triton X-100 and the polarized distribution of apical (pcx, gp114, PLAP) and basolateral (p58, E-cadherin) membrane markers was analyzed by immunofluorescence. All of the apical and basolateral markers tested were correctly localized to their target membranes in cav1-KD cells.

majority of the caveolin-2 staining was found to extensively colocalize with giantin, a Golgi marker, whereas the plasma membrane pool of caveolin-2 was strongly reduced (Fig. 4A). This phenomenon was even more prominent when an adenovirus expressing canine caveolin-2 fused to GFP (GFP-cav2) was used to follow the biosynthetic delivery of caveolin-2. Sixteen hours after infection, caveolin-2 colocalized with caveolin-1 at the basolateral membrane in the control cells (Fig. 4B and C). In addition, a small intracellular pool of EGFP-cav2 was observed. In cav1-KD cells, essentially no GFP-cav2 was delivered to the plasma membrane during the 16 h following the infection and the GFP-cav2 was found in the Golgi apparatus instead (Fig. 4B and C). Thus, caveolin-2 fails to enter the basolateral trafficking pathway in caveolin-1-depleted MDCK cells and is retained in the Golgi. Taken together, our observations validate the use of these cells as a true caveolin-1-negative model system.

Kinetics of apical transport are not affected in Cav-1-depleted MDCK cells. In contrast to the proposed role of caveolin-1 as a key component of the apical transport machinery, all of the apical membrane markers tested, including the GPI-anchored PLAP, were correctly polarized in filter-grown cav1-KD MDCK cells. Nevertheless, a transient perturbation in apical transport might be overlooked in such a steady-state assay. To analyze the kinetics of apical transport, we used a well-established hemagglutinin transport assay. This quantitative assay measures the surface arrival of an apically targeted HA envelope protein of influenza virus. The same assay was also used in the previous study where caveolin-1 antibodies were shown to inhibit HA-transport in MDCK cells (56). However, we did not observe any kinetic differences in the surface arrival of HA in control and in cav1-KD cells (Fig. 5A). Disruption of microtubular networks by nocodazole-treatment, on the other hand, effectively perturbed apical transport as expected (20, 26). Because of the very similar kinetics of HA transport in control and in cav1-KD cells it is unlikely that HA in cav1-KD cells would reach the apical surface via another pathway, such as transcytosis.

To study the kinetics of GPI-anchored protein transport we infected control and cav1-KD MDCK cells with a PLAP-expressing adenovirus. Cells were metabolically labeled and the surface transport of PLAP was quantitated using a surface biotinylation assay. In line with our observations from the HA transport assay, we found that the transport kinetics of PLAP were similar in control and in cav1-KD cells (Fig. 5B). In addition, no significant differences were seen when another GPI-anchored marker, yellow fluorescent protein fused to a GPI-anchor (YFP-GL-GPI) (24) was used (data not shown). Thus, our data demonstrate that caveolin-1 is not required for the efficient surface delivery of HA or of GPI-anchored proteins in MDCK cells.

Surface expression of GPI-anchored proteins in Cav1-KO-derived mouse embryonic fibroblasts. A previous study reported a block in the surface delivery of GPI-anchored proteins in cells derived from the cav1-KO mice (60). To assess the contribution of the different cell types, we analyzed the transport kinetics of PLAP in immortalized mouse embryonic fibroblasts derived from cav1-KO mice (10). MEFs were infected with PLAP-adenovirus and analyzed by immunofluorescence without permeabilization to specifically label PLAP on the cell surface. In accordance to our data from cav1-KD MDCK cells, we observed a robust PLAP signal on the cell surface of cav1-KO MEFs (Fig. 6A). Similar results were observed in primary MEF cultures and in primary lung fibroblasts isolated from cav1-KO mice (data not shown). Exposure of PLAP at the cell surface was confirmed by a surface biotinylation experiment in pulse-labeled MEFs (Fig. 6B).

To confirm that also the endogenous GPI-anchored proteins are delivered to the cell surface we employed the properties of aerolysin, a bacterial toxin that binds to GPI-anchors (9). We used a fluorophore-conjugated non-pore-forming mutant of aerolysin (Alexa-546-ASSP) (14) to label the GPI-anchored proteins. In permeabilized wild-type (wild-type) and cav1-KO MEFs, perinuclear, as well as plasma membrane staining was observed (Fig. 6C). When we probed unpermeabilized wild-type and cav1-KO MEFs with Alexa-546-ASSP, in both cases a

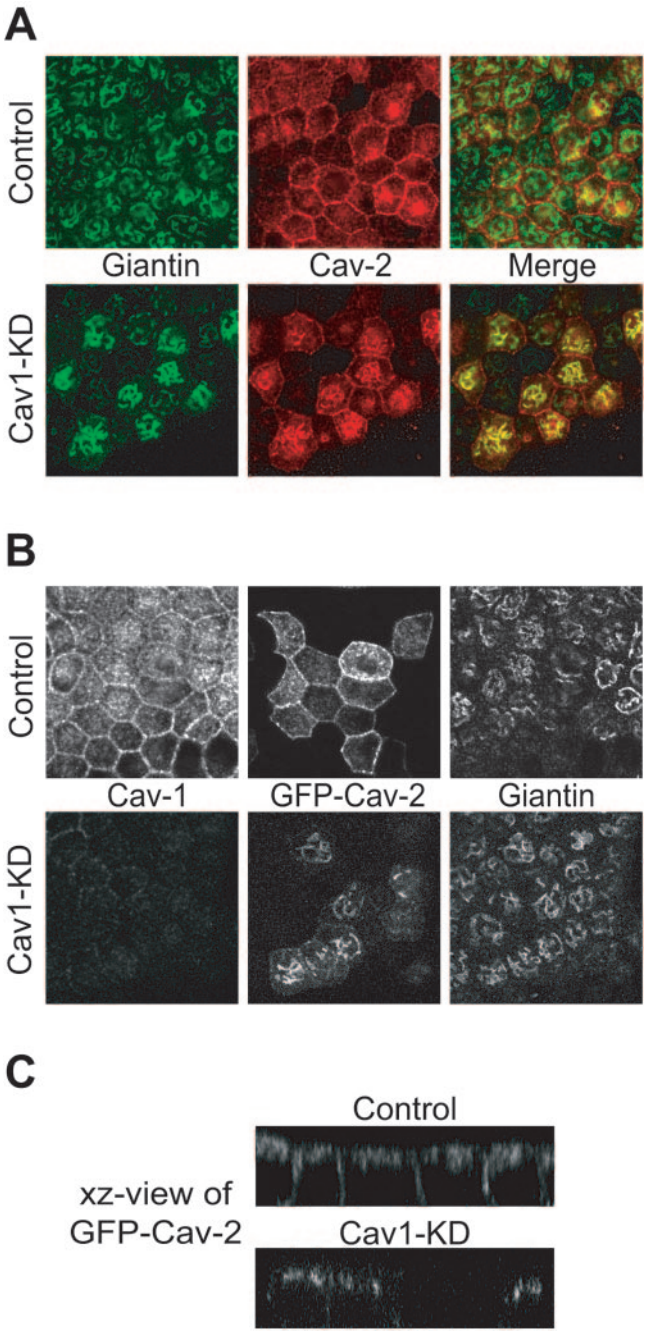

FIG. 4. Caveolin-2 is retained in the Golgi apparatus in cav1-KD MDCK cells. (A) Control and cav1-KD MDCK cells were grown on Transwell filters for 3 days. Cells were fixed with paraformaldehyde, permeabilized with saponin and immunostained using giantin and caveolin-2 antibodies to visualize the Golgi apparatus and endogenous caveolin-2, respectively. In control cells caveolin-2 was mainly localized at the basolateral membrane. An intracellular perinuclear staining was also seen. In cav1-KD MDCK cells caveolin-2 accumulated in the Golgi, whereas the plasma membrane pool was strongly reduced. (B) Control and cav1-KD cells were grown on filters for 2 days followed by an infection with an adenovirus expressing GFP-cav2 fusion protein. Sixteen hours later, cells were fixed, permeabilized with saponin, and immunostained using antibodies against caveolin-1 and giantin. In control cells GFP-cav2 was found at the basolateral membrane with some additional perinuclear/subapical intracellular staining. In cav1-KD cells, basolateral staining was not observed and GFP-cav2 was retained in the Golgi. (C) xz view of GFP-cav2 in filter-grown control and cav1-KD MDCK cells.

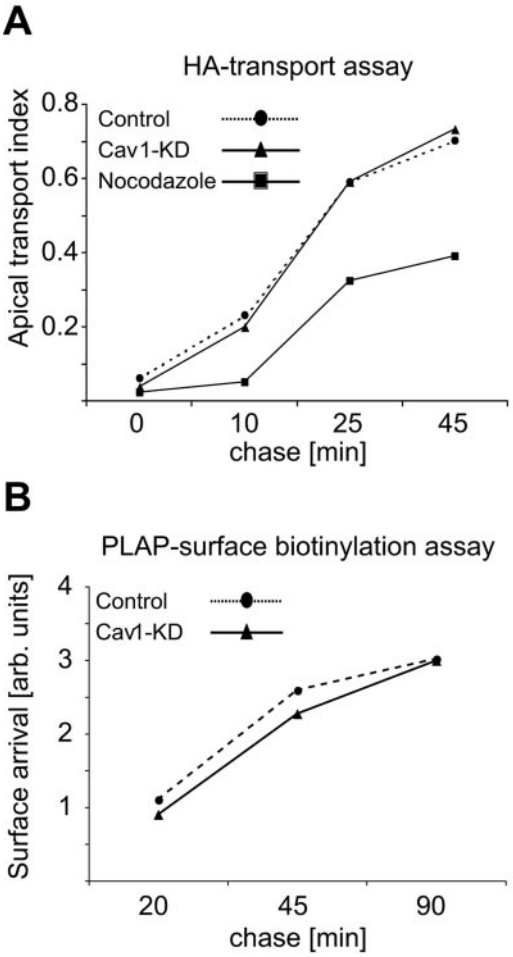

FIG. 5. Surface delivery of HA and PLAP is unaffected in cav1-KD MDCK cells. (A) Filter-grown (day 3) control and cav1-KD cells were infected with fowl plague virus and pulsed with [^{35}S]methionine. Cells were incubated at 19.5°C to accumulate biosynthetic cargo at the trans-Golgi network, after which the cargo was released and chased for the indicated times at 37°C. The apical surface-exposed HA was quantified as described in Materials and Methods. (B) Filter-grown (days 2 to 3) control and cav1-KD cells were infected with an adenovirus expressing PLAP for 16 h. Cells were pulsed with [^{35}S]methionine and chased for the indicated times. Cell surface proteins were biotinylated and the surface-delivered PLAP was quantified as described in Materials and Methods. The data shown are representative of three (HA) and four (PLAP) independent experiments.

surface staining of roughly similar intensity was detected (Fig. 6C). In conclusion, like in cav1-depleted MDCK cells, we observed neither a block nor a significant delay in the surface delivery of GPI-anchored proteins in cav1-KO mouse-derived fibroblasts.

To study the role of caveolin-1 in the surface delivery of an endogenous GPI-anchored protein in polarized tissue in vivo, we compared the localization of Tamm-Horsfall protein in the kidney sections from wild-type and cav1-KO mice. Tamm-Horsfall protein is a GPI-anchored glycoprotein that is highly expressed on the apical plasma membrane of the renal tubular epithelial cells (55). In agreement with our findings from cav1-KD MDCK cells and from cav1-KO MEFs, we observed

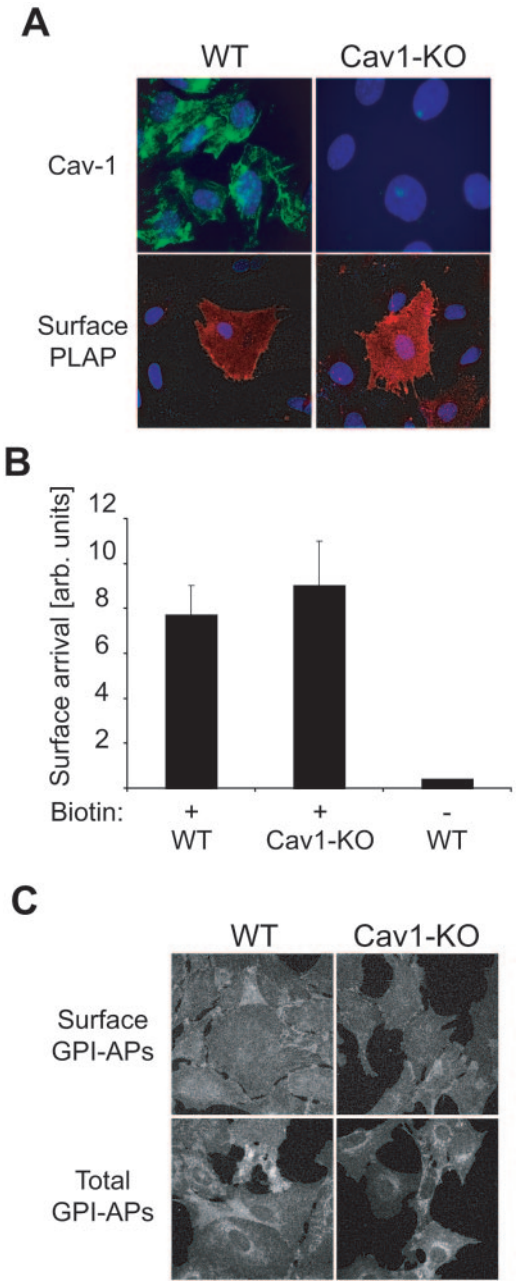

FIG. 6. GPI-anchored proteins are transported to the cell surface in immortalized mouse embryonic fibroblasts derived from the cav1-KO mice. (A) Coverslip-grown wild-type (wild-type) and cav1-KO MEFs were infected with a PLAP-expressing adenovirus. Ten hours later, cells were fixed and PLAP and caveolin-1 were visualized by immunofluorescence in unpermeabilized (PLAP) or saponin-permeabilized (caveolin-1) cells. Nuclei were stained with 4′,6′-diamidino-2-phenylindole (DAPI). (B) Wild-type and cav1-KO MEFs were infected with PLAP-expressing adenovirus for 16 h. Cells were pulsed with [^{35}S]methionine for 15 min and chased for 60 min. Surface-exposed PLAP was biotinylated and quantified as described in Materials and Methods. The data shown come from three independent experiments (C) Wild-type and cav1-KO MEFs were grown on coverslips and fixed, and surface-exposed GPI-anchored proteins (GPI-APs) were labeled using an Alexa 546-conjugated aerolysin mutant (Alexa-546-ASSP) on unpermeabilized cells. Total GPI-anchored protein signal was visualized in paraformaldehyde-fixed, saponin-permeabilized MEFs.

no difference in the subcellular localization of Tamm-Horsfall protein between the wild-type and the cav1-KO mice (Fig. 7).

DISCUSSION

In this study, we have examined the role of caveolin-1 in the apical transport pathway by using RNAi to specifically deplete caveolin-1 expression in a well-characterized polarized cell model system, MDCK cells. The cav1-KD MDCK cells lacked caveolae but formed polarized monolayers when grown on a filter support. The kinetics of the surface delivery of HA and PLAP were not affected in cav1-KD cells. Our data clearly showed that caveolin-1 is not an essential component of the apical transport machinery in MDCK cells. This result is in agreement with earlier findings from Fischer rat thyroid (FRT) cells (30) but seemingly contradictory to a report from our laboratory, where HA transport to the apical surface was perturbed upon application of intracellular caveolin-1 antibodies to permeabilized MDCK cells (56). However, basolateral transport was not affected.

A recent study by Parton and coworkers offers a possible explanation for this differential inhibition (49). Certain antibodies against caveolin-1 were found to preferentially recognize the plasma membrane pool, whereas other antibodies only labeled the Golgi pool of caveolin-1. The antibody used by Scheiffele et al. was found to belong to the former category. We speculate that this antibody recognized the conformation of caveolin-1 in the apically targeted large homo-oligomers, whereas the basolaterally targeted caveolin-1 in caveolin-1/2 hetero-oligomers was not efficiently captured. Such a difference might explain the seemingly specific inhibition of the apical but not the basolateral trafficking pathway. Thus, in light of our results, it seems likely that the inhibition observed in the previous study was due to steric hindrance of the apical transport machinery by the caveolin-1 antibodies bound to high-molecular-weight caveolin-1 oligomers (56).

Our data do not support the conclusion of Lisanti and coworkers, who reported that the transport of GPI-anchored proteins to the cell surface is blocked in cav1-KO cells (60). We excluded that cell type-specific effects were responsible for the different results by showing that the biosynthetic transport of GPI-anchored proteins was not dependent on caveolin-1 in an essentially identical cell model, cav1-KO mouse-derived MEFs. One difference between these two studies was the method used to detect endogenous GPI-anchored proteins. Although both approaches were based on aerolysin, we utilized an aerolysin mutant directly conjugated to a fluorophore, whereas Sotgia et al. used a detection system based on an aerolysin antibody (Protox Biotech). In our hands this aerolysin antibody was not suitable for immunofluorescence, as we detected only very weak staining even in cells highly overexpressing an exogenous GPI-anchored marker protein (data not shown).

Additionally, it could be speculated that the immortalized MEFs used in these two studies represent populations with different properties. However, this is unlikely, as several other phenotypes reported for MEFs used by Sotgia et al. (for example, enhanced growth rate and intracellular accumulation of caveolin-2) were also found in the MEFs used in this study (S. Le Lay and T. V. Kurzchalia, unpublished results). In addition,

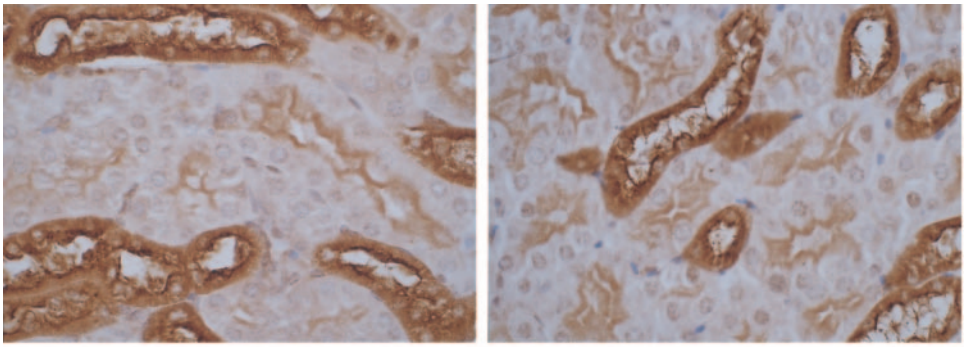

FIG. 7. Tamm-Horsfall protein, an endogenous GPI-anchored protein, is localized to the apical membrane of the kidney tubules in both wild-type and cav1-KO mice. Paraffin-embedded kidney sections from wild-type and cav1-KO mice were stained using antibody against Tamm-Horsfall protein. The sections were counterstained with hematoxylin. Three wild-type and three cav1-KO mice were analyzed.

we also observed normal PLAP trafficking in primary nonimmortalized cav1-KO fibroblasts (passage <5, data not shown).

Importantly, we found that Tamm-Horsfall protein, an endogenous GPI-anchored protein, was localized at the apical surface of renal tubular epithelial cells in both the wild-type and the cav1-KO mice. The same protein was reported to accumulate intracellularly in the previous study (60). We do not know the reason for the different results. Finally, given the relatively mild phenotype of the cav1-KO mice (10, 52, 65) in comparison with the severe consequences resulting even upon a tissue-specific knockout of GPI-anchored proteins (1, 23, 40, 61) the suggested essential role for caveolin-1 in the surface delivery of GPI-anchored proteins seems unlikely. We cannot of course exclude that caveolin-1 indeed participates in apical sorting and delivery but is replaced by other proteins in caveolin-1-depleted cells.

Although caveolin-1 is dispensable for general biosynthetic delivery of apical membrane cargo, it appears to play a role in the surface transport of caveolin-2 (35, 43), angiotensin receptor (63), and the TRPC-1 receptor (3). Here, we confirmed in our model system that efficient basolateral transport of caveolin-2 depends on the presence of caveolin-1.

What then might be the function of caveolins in cells? Clearly, caveolin and caveolae have a role in down-regulation of endothelial nitric oxide synthase (10, 52). A number of studies have established a connection between caveolins and lipid droplets, neutral lipid-filled organelles surrounded by a phospholipid monolayer (16, 42, 47). Importantly, external modulation of the cellular lipid homeostasis affects the targeting of caveolins to lipid droplets (48, 49). Moreover, caveolin-1 expression is positively regulated by an increase in cellular cholesterol levels (reviewed in reference 13) and cholesterol transport to the lipid droplets is altered in Cav1-KO MEFs differentiated into adipocytes (S. Le Lay et al., submitted). A role for caveolin-1 as a regulator of lipid homeostasis is further supported by the lean phenotype of the cav1-KO mice exposed to a high-fat diet (51). Parton and colleagues have suggested an attractive model in which caveolin acts as a sensor in regulation of the cellular cholesterol levels (49). How such a regulatory mechanism would function to guide cellular cholesterol transport is not known.

Whether or not caveolins regulate lipid homeostasis, caveolae are likely to be central for caveolin function. Caveolae could function as storage organelles for raft components, harboring cholesterol and sphingolipids for cellular use. Mobilization of caveolae is triggered by viruses such as simian virus 40 (46) but presumably also by natural ligands not yet identified. In retrograde transport caveolar units form highly mobile but structurally stable sorting platforms for endocytic cargo (44). What cargo caveolae normally transport and where the cargo is delivered are open issues, which must be tackled before the cellular role of caveolins will be fully understood.

ACKNOWLEDGMENTS

Stephanie Dienel and Jana Mäntler are acknowledged for expert technical assistance. We thank Marek Drab for help with primary mouse lung fibroblasts.

A.M. is a recipient of an EMBO Long-Term Fellowship (ALTF-50-2002). S.L.L. is a Marie Curie Fellow, contract no. MEIF-CT-2003-500768.

REFERENCES

1. **Alfieri, J. A., A. D. Martin, J. Takeda, G. Kondoh, D. G. Myles, and P. Primakoff.** 2003. Infertility in female mice with an oocyte-specific knockout of GPI-anchored proteins. J. Cell Sci. **116:**2149–2155.
2. **Balcarova-Stander, J., S. E. Pfeiffer, S. D. Fuller, and K. Simons.** 1984. Development of cell surface polarity in the epithelial Madin-Darby canine kidney (MDCK) cell line. EMBO J. **3:**2687–2694.
3. **Brazer, S. C., B. B. Singh, X. Liu, W. Swaim, and I. S. Ambudkar.** 2003. Caveolin-1 contributes to assembly of store-operated Ca^{2+} influx channels by regulating plasma membrane localization of TRPC1. J. Biol. Chem. **278:** 27208–27215.
4. **Brown, D. A., B. Crise, and J. K. Rose.** 1989. Mechanism of membrane anchoring affects polarized expression of two proteins in MDCK cells. Science **245:**1499–1501.
5. **Cheong, K. H., D. Zacchetti, E. E. Schneeberger, and K. Simons.** 1999. VIP17/MAL, a lipid raft-associated protein, is involved in apical transport in MDCK cells. Proc. Natl. Acad. Sci. USA **96:**6241–6248.
6. **Cohen, A. W., R. Hnasko, W. Schubert, and M. P. Lisanti.** 2004. Role of caveolae and caveolins in health and disease. Physiol. Rev. **84:**1341–1379.
7. **Delacour, D., V. Gouyer, J. P. Zanetta, H. Drobecq, E. Leteurtre, G. Grard, O. Moreau-Hannedouche, E. Maes, A. Pons, S. Andre, A. Le Bivic, H. J. Gabius, A. Manninen, K. Simons, and G. Huet.** 2005. Galectin-4 and sulfatides in apical membrane trafficking in enterocyte-like cells. J. Cell Biol. **169:**491–501.
8. **de Marco, M. C., F. Martin-Belmonte, L. Kremer, J. P. Albar, I. Correas, J. P. Vaerman, M. Marazuela, J. A. Byrne, and M. A. Alonso.** 2002. MAL2, a novel raft protein of the MAL family, is an essential component of the machinery for transcytosis in hepatoma HepG2 cells. J. Cell Biol. **159:**37–44.
9. **Diep, D. B., K. L. Nelson, S. M. Raja, E. N. Pleshak, and J. T. Buckley.** 1998. Glycosylphosphatidylinositol anchors of membrane glycoproteins are binding determinants for the channel-forming toxin aerolysin. J. Biol. Chem. **273:**2355–2360.

10. **Drab, M., P. Verkade, M. Elger, M. Kasper, M. Lohn, B. Lauterbach, J. Menne, C. Lindschau, F. Mende, F. C. Luft, A. Schedl, H. Haller, and T. V. Kurzchalia.** 2001. Loss of caveolae, vascular dysfunction, and pulmonary defects in caveolin-1 gene-disrupted mice. Science **293:**2449–2452.
11. **Etienne-Manneville, S., and A. Hall.** 2003. Cell polarity: Par6, aPKC and cytoskeletal crosstalk. Curr. Opin. Cell Biol. **15:**67–72.
12. **Fiedler, K., F. Lafont, R. G. Parton, and K. Simons.** 1995. Annexin XIIIb: a novel epithelial specific annexin is implicated in vesicular traffic to the apical plasma membrane. J. Cell Biol. **128:**1043–1053.
13. **Fielding, C. J., and P. E. Fielding.** 2000. Cholesterol and caveolae: structural and functional relationships. Biochim. Biophys. Acta **1529:**210–222.
14. **Fivaz, M., F. Vilbois, S. Thurnheer, C. Pasquali, L. Abrami, P. E. Bickel, R. G. Parton, and F. G. Van Der Goot.** 2002. Differential sorting and fate of endocytosed GPI-anchored proteins. EMBO J. **21:**3989–4000.
15. **Fra, A. M., E. Williamson, K. Simons, and R. G. Parton.** 1995. De novo formation of caveolae in lymphocytes by expression of VIP21-caveolin. Proc. Natl. Acad. Sci. USA **92:**8655–8659.
16. **Fujimoto, T., H. Kogo, K. Ishiguro, K. Tauchi, and R. Nomura.** 2001. Caveolin-2 is targeted to lipid droplets, a new "membrane domain" in the cell. J. Cell Biol. **152:**1079–1085.
17. **Fujimoto, T., H. Kogo, R. Nomura, and T. Une.** 2000. Isoforms of caveolin-1 and caveolar structure. J. Cell Sci. **113:**3509–3517.
18. **Fullekrug, J., P. Scheiffele, and K. Simons.** 1999. VIP36 localisation to the early secretory pathway. J. Cell Sci. **112:**2813–2821.
19. **Fullekrug, J., and K. Simons.** 2004. Lipid rafts and apical membrane traffic. Ann. N. Y. Acad. Sci. **1014:**164–169.
20. **Gilbert, T., A. Le Bivic, A. Quaroni, and E. Rodriguez-Boulan.** 1991. Microtubular organization and its involvement in the biogenetic pathways of plasma membrane proteins in Caco-2 intestinal epithelial cells. J. Cell Biol. **113:**275–288.
21. **Gumbiner, B., and K. Simons.** 1986. A functional assay for proteins involved in establishing an epithelial occluding barrier: identification of a uvomorulin-like polypeptide. J. Cell Biol. **102:**457–468.
22. **Hara-Kuge, S., A. Seko, O. Shimada, H. Tosaka-Shimada, and K. Yamashita.** 2004. The binding of VIP36 and alpha-amylase in the secretory vesicles via high-mannose type glycans. Glycobiology **14:**739–744.
23. **Kawagoe, K., D. Kitamura, M. Okabe, I. Taniuchi, M. Ikawa, T. Watanabe, T. Kinoshita, and J. Takeda.** 1996. Glycosylphosphatidylinositol-anchor-deficient mice: implications for clonal dominance of mutant cells in paroxysmal nocturnal hemoglobinuria. Blood **87:**3600–3606.
24. **Keller, P., D. Toomre, E. Diaz, J. White, and K. Simons.** 2001. Multicolour imaging of post-Golgi sorting and trafficking in live cells. Nat. Cell Biol. **3:**140–149.
25. **Kurzchalia, T. V., P. Dupree, R. G. Parton, R. Kellner, H. Virta, M. Lehnert, and K. Simons.** 1992. VIP21, a 21-kD membrane protein is an integral component of trans-Golgi-network-derived transport vesicles. J. Cell Biol. **118:**1003–1014.
26. **Lafont, F., J. K. Burkhardt, and K. Simons.** 1994. Involvement of microtubule motors in basolateral and apical transport in kidney cells. Nature **372:**801–803.
27. **Lafont, F., S. Lecat, P. Verkade, and K. Simons.** 1998. Annexin XIIIb associates with lipid microdomains to function in apical delivery. J. Cell Biol. **142:**1413–1427.
28. **Lahtinen, U., M. Honsho, R. G. Parton, K. Simons, and P. Verkade.** 2003. Involvement of caveolin-2 in caveolar biogenesis in MDCK cells. FEBS Lett. **538:**85–88.
29. **Linstedt, A. D., and H. P. Hauri.** 1993. Giantin, a novel conserved Golgi membrane protein containing a cytoplasmic domain of at least 350 kDa. Mol. Biol. Cell **4:**679–693.
30. **Lipardi, C., R. Mora, V. Colomer, S. Paladino, L. Nitsch, E. Rodriguez-Boulan, and C. Zurzolo.** 1998. Caveolin transfection results in caveolae formation but not apical sorting of glycosylphosphatidylinositol (GPI)-anchored proteins in epithelial cells. J. Cell Biol. **140:**617–626.
31. **Liu, P., M. Rudick, and R. G. Anderson.** 2002. Multiple functions of caveolin-1. J. Biol. Chem. **277:**41295–41298.
32. **Matlin, K. S., and K. Simons.** 1983. Reduced temperature prevents transfer of a membrane glycoprotein to the cell surface but does not prevent terminal glycosylation. Cell **34:**233–243.
33. **Meder, D., A. Shevchenko, K. Simons, and J. Fullekrug.** 2005. Gp135/podocalyxin and NHERF-2 participate in the formation of a preapical domain during polarization of MDCK cells. J. Cell Biol. **168:**303–313.
34. **Monier, S., R. G. Parton, F. Vogel, J. Behlke, A. Henske, and T. V. Kurzchalia.** 1995. VIP21-caveolin, a membrane protein constituent of the caveolar coat, oligomerizes in vivo and in vitro. Mol. Biol. Cell. **6:**911–927.
35. **Mora, R., V. L. Bonilha, A. Marmorstein, P. E. Scherer, D. Brown, M. P. Lisanti, and E. Rodriguez-Boulan.** 1999. Caveolin-2 localizes to the golgi complex but redistributes to plasma membrane, caveolae, and rafts when co-expressed with caveolin-1. J. Biol. Chem. **274:**25708–25717.
36. **Mostov, K., T. Su, and M. ter Beest.** 2003. Polarized epithelial membrane traffic: conservation and plasticity. Nat. Cell Biol. **5:**287–293.
37. **Murata, M., J. Peranen, R. Schreiner, F. Wieland, T. V. Kurzchalia, and K. Simons.** 1995. VIP21/caveolin is a cholesterol-binding protein. Proc. Natl. Acad. Sci. USA **92:**10339–10343.
38. **Nakatsu, F., and H. Ohno.** 2003. Adaptor protein complexes as the key regulators of protein sorting in the post-Golgi network. Cell Struct. Funct. **28:**419–429.
39. **Nelson, W. J.** 2003. Adaptation of core mechanisms to generate cell polarity. Nature **422:**766–774.
40. **Nozaki, M., K. Ohishi, N. Yamada, T. Kinoshita, A. Nagy, and J. Takeda.** 1999. Developmental abnormalities of glycosylphosphatidylinositol-anchor-deficient embryos revealed by Cre/loxP system. Lab. Investig. **79:**293–299.
41. **Ojakian, G. K., and R. Schwimmer.** 1988. The polarized distribution of an apical cell surface glycoprotein is maintained by interactions with the cytoskeleton of Madin-Darby canine kidney cells. J. Cell Biol. **107:**2377–2387.
42. **Ostermeyer, A. G., J. M. Paci, Y. Zeng, D. M. Lublin, S. Munro, and D. A. Brown.** 2001. Accumulation of caveolin in the endoplasmic reticulum redirects the protein to lipid storage droplets. J. Cell Biol. **152:**1071–1078.
43. **Parolini, I., M. Sargiacomo, F. Galbiati, G. Rizzo, F. Grignani, J. A. Engelman, T. Okamoto, T. Ikezu, P. E. Scherer, R. Mora, E. Rodriguez-Boulan, C. Peschle, and M. P. Lisanti.** 1999. Expression of caveolin-1 is required for the transport of caveolin-2 to the plasma membrane. Retention of caveolin-2 at the level of the golgi complex. J. Biol. Chem. **274:**25718–25725.
44. **Pelkmans, L., T. Burli, M. Zerial, and A. Helenius.** 2004. Caveolin-stabilized membrane domains as multifunctional transport and sorting devices in endocytic membrane traffic. Cell **118:**767–780.
45. **Pelkmans, L., and A. Helenius.** 2002. Endocytosis via caveolae. Traffic **3:**311–320.
46. **Pelkmans, L., D. Puntener, and A. Helenius.** 2002. Local actin polymerization and dynamin recruitment in SV40-induced internalization of caveolae. Science **296:**535–539.
47. **Pol, A., R. Luetterforst, M. Lindsay, S. Heino, E. Ikonen, and R. G. Parton.** 2001. A caveolin dominant negative mutant associates with lipid bodies and induces intracellular cholesterol imbalance. J. Cell Biol. **152:**1057–1070.
48. **Pol, A., S. Martin, M. A. Fernandez, C. Ferguson, A. Carozzi, R. Luetterforst, C. Enrich, and R. G. Parton.** 2004. Dynamic and regulated association of caveolin with lipid bodies: modulation of lipid body motility and function by a dominant negative mutant. Mol. Biol. Cell. **15:**99–110.
49. **Pol, A., S. Martin, M. A. Fernandez, M. Ingelmo-Torres, C. Ferguson, C. Enrich, and R. G. Parton.** 2005. Cholesterol and fatty acids regulate dynamic caveolin trafficking through the golgi complex and between the cell surface and lipid bodies. Mol. Biol. Cell **16:**2091–2105.
50. **Puertollano, R., F. Martin-Belmonte, J. Millan, M. C. de Marco, J. P. Albar, L. Kremer, and M. A. Alonso.** 1999. The MAL proteolipid is necessary for normal apical transport and accurate sorting of the influenza virus hemagglutinin in Madin-Darby canine kidney cells. J. Cell Biol. **145:**141–151.
51. **Razani, B., T. P. Combs, X. B. Wang, P. G. Frank, D. S. Park, R. G. Russell, M. Li, B. Tang, L. A. Jelicks, P. E. Scherer, and M. P. Lisanti.** 2002. Caveolin-1-deficient mice are lean, resistant to diet-induced obesity, and show hypertriglyceridemia with adipocyte abnormalities. J. Biol. Chem. **277:**8635–8647.
52. **Razani, B., J. A. Engelman, X. B. Wang, W. Schubert, X. L. Zhang, C. B. Marks, F. Macaluso, R. G. Russell, M. Li, R. G. Pestell, D. Di Vizio, H. Hou, Jr., B. Kneitz, G. Lagaud, G. J. Christ, W. Edelmann, and M. P. Lisanti.** 2001. Caveolin-1 null mice are viable but show evidence of hyperproliferative and vascular abnormalities. J. Biol. Chem. **276:**38121–38138.
53. **Rodriguez-Boulan, E., G. Kreitzer, and A. Musch.** 2005. Organization of vesicular trafficking in epithelia. Nat. Rev. Mol. Cell. Biol. **6:**233–247.
54. **Rothberg, K. G., J. E. Heuser, W. C. Donzell, Y. S. Ying, J. R. Glenney, and R. G. Anderson.** 1992. Caveolin, a protein component of caveolae membrane coats. Cell **68:**673–682.
55. **Saemann, M. D., T. Weichhart, W. H. Horl, and G. J. Zlabinger.** 2005. Tamm-Horsfall protein: a multilayered defence molecule against urinary tract infection. Eur. J. Clin. Investig. **35:**227–235.
56. **Scheiffele, P., P. Verkade, A. M. Fra, H. Virta, K. Simons, and E. Ikonen.** 1998. Caveolin-1 and -2 in the exocytic pathway of MDCK cells. J. Cell Biol. **140:**795–806.
57. **Schuck, S., A. Manninen, M. Honsho, J. Fullekrug, and K. Simons.** 2004. Generation of single and double knockdowns in polarized epithelial cells by retrovirus-mediated RNA interference. Proc. Natl. Acad. Sci. USA **101:**4912–4917.
58. **Schuck, S., and K. Simons.** 2004. Polarized sorting in epithelial cells: raft clustering and the biogenesis of the apical membrane. J. Cell Sci. **117:**5955–5964.
59. **Simons, K., and W. L. Vaz.** 2004. Model systems, lipid rafts, and cell membranes. Annu. Rev. Biophys. Biomol. Struct. **33:**269–295.
60. **Sotgia, F., B. Razani, G. Bonuccelli, W. Schubert, M. Battista, H. Lee, F. Capozza, A. L. Schubert, C. Minetti, J. T. Buckley, and M. P. Lisanti.** 2002. Intracellular retention of glycosylphosphatidyl inositol-linked proteins in caveolin-deficient cells. Mol. Cell. Biol. **22:**3905–3926.
61. **Tarutani, M., S. Itami, M. Okabe, M. Ikawa, T. Tezuka, K. Yoshikawa, T. Kinoshita, and J. Takeda.** 1997. Tissue-specific knockout of the mouse Pig-a gene reveals important roles for GPI-anchored proteins in skin development. Proc. Natl. Acad. Sci. USA **94:**7400–7405.

62. **Verkade, P., T. Harder, F. Lafont, and K. Simons.** 2000. Induction of caveolae in the apical plasma membrane of Madin-Darby canine kidney cells. J. Cell Biol. **148:**727–739.
63. **Wyse, B. D., I. A. Prior, H. Qian, I. C. Morrow, S. Nixon, C. Muncke, T. V. Kurzchalia, W. G. Thomas, R. G. Parton, and J. F. Hancock.** 2003. Caveolin interacts with the angiotensin II type 1 receptor during exocytic transport but not at the plasma membrane. J. Biol. Chem. **278:**23738–23746.
64. **Yoshimori, T., P. Keller, M. G. Roth, and K. Simons.** 1996. Different biosynthetic transport routes to the plasma membrane in BHK and CHO cells. J. Cell Biol. **133:**247–256.
65. **Zhao, Y. Y., Y. Liu, R. V. Stan, L. Fan, Y. Gu, N. Dalton, P. H. Chu, K. Peterson, J. Ross, Jr., and K. R. Chien.** 2002. Defects in caveolin-1 cause dilated cardiomyopathy and pulmonary hypertension in knockout mice. Proc. Natl. Acad. Sci. USA **99:**11375–11380.